Fine Grained Silicon-Tungsten Calorimetry for a Linear Collider Detector

D. Strom, R. Frey, M. Breidenbach, D. Freytag, N. Graf, G. Haller, O. Milgrome, and V. Radeka

***Abstract*—A fine grained silicon-tungsten calorimeter is ideal for use as the electromagnetic calorimeter in a linear collider detector optimized for particle-flow reconstruction. We are designing a calorimeter that is based on readout chips which are bump bonded to the silicon wafers that serve as the active medium in the calorimeter. By using integrated electronics we plan to demonstrate that fine granularity can be achieved at a reasonable price. Our design minimizes the gap between tungsten layers leading to a small Molière radius, an important figure of merit for particle-flow detectors. Tests of the silicon detectors to be used in a test beam prototype as well as timing measurements based onsimilar silicon detectors are discussed.**

***Index Terms*—Calorimetry, energy measurement, position sensitive particle detectors, silicon radiation detectors, time measurement, tungsten.**

I. Introduction

THE properties of the electromagnetic calorimeter in a general purpose detector designed for use at a TeV Linear Collider (LC) are likely to drive the design of much of the rest of the detector. The main role of the electromagnetic calorimeter is to cleanly separate energy deposits from photons from those due to charged particles. In hadronic jets this allows the energy associated with the charged particles to be accurately measured in the tracker and electromagnetic showers due to photons to be measured in the electromagnetic calorimeter. To complete the hadronic jet energy measurement, the energy due to neutral hadrons must be separated from the energy deposited by charged hadrons and photons in both the electromagnetic and hadron calorimeters. A very granular detector [1] allows for a true particle-flow measurement as opposed to LEP era energy-flow measurements which mainly corrected for double counting in merged clusters of photons and charged hadrons [2].

The design of the electromagnetic calorimeter drives the design of the remaining subsystems in several ways. To provide unambiguous particle-flow measurement it is advantageous to have both the electromagnetic and hadron calorimeters located inside the coil. Thus if the calorimeter can be made sufficiently dense it is possible to reduce the radius of the calorimeter while maintaining the same performance. This in turn can reduce the size of the hadron calorimeter and stored energy in the magnetic field.

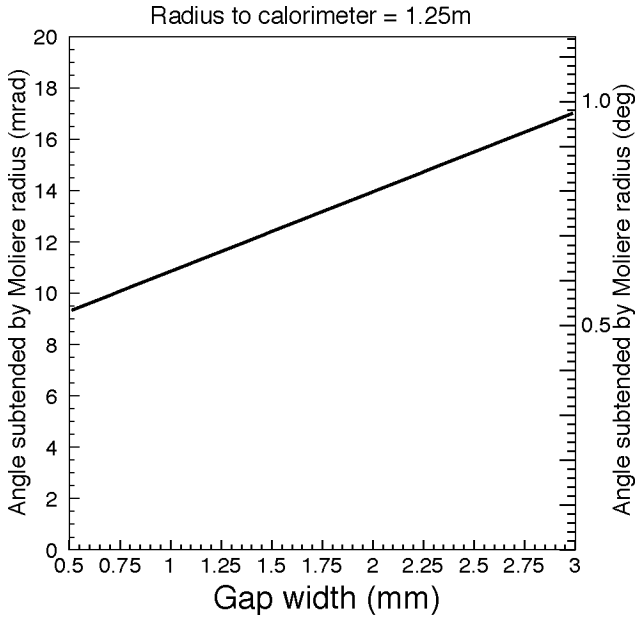

Fig. 1. Angle subtended by the effective Molière radius versus gap size for 2.5 mm 92.5% tungsten plates. It is assumed that the Molière radius scales as the overall density of the calorimeter.

In our design we use nonmagnetic tungsten alloy (92.5% W, 6.6% Fe, 0.9% Ni, $\rho = 17.7\ \mathrm{g/cm^3}$) absorber and 300 μm silicon detectors as an active medium. To keep the overall calorimeter as dense as possible we try to minimize the gap between layers. Fig. 1 shows the angle subtended by the effective Molière radius as a function of the distance between tungsten alloy layers 2.5 mm thick. A possible cross section for the detector is shown in Fig. 2. The main challenges for the detector builder is to develop a system of detector readout which does not require excessive gap space for cooling and electronics.

More details of the proposed detector can be found in [3] and [4]. In this report we concentrate on laboratory measurements of prototype silicon detectors and on timing measurements with silicon pad detectors.

Manuscript received November 8, 2004; revised April 8, 2005. This work was supported in part by the U.S. Department of Energy.

D. Strom and R. Frey are with the University of Oregon, Eugene, OR 97403 USA (e-mail: strom@physics.uoregon.edu; rayfrey@cosmic.uoregon.edu).

M. Breidenbach, D. Freytag, N. Graf, G. Haller, and O. Milgrome are with Stanford Linear Accelerator Center, Stanford, CA 94309 USA (e-mail: mib@slac.stanford.edu; drf@slac.stanford.edu; ngraf@slac.stanford.edu; haller@slac.stanford.edu).

V. Radeka is with Brookhaven National Laboratory, Upton, NY 11973 USA (e-mail: Radeka@bnl.gov).

Submitted to IEEE Trans.Nucl.Sci.

Work supported in part by Department of Energy contract DE-AC02-76SF00515

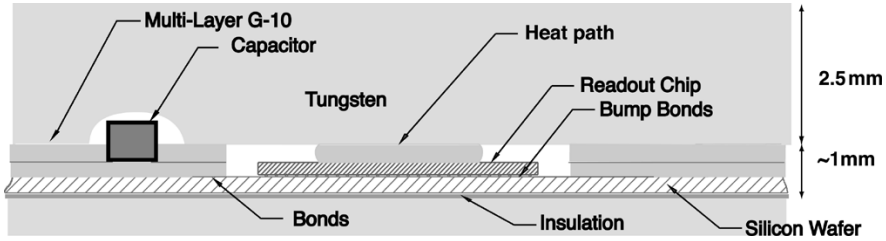

Fig. 2. Possible cross section showing the active silicon detector, the readout chip and the PC board used to connect the readout chip to power and the DAQ system.

A. Impact of Accelerator Design on Detector Design

Two very different technologies for LC accelerators have been proposed. The "warm" option, based on X-band RF room temperature cavities, implies short bunch trains with 192 bunches separated by 1.4 ns repeated at 120 Hz. The "cold" option, based on L-band superconducting cavities, implies longer bunch trains with 2820 bunches separated by 337 ns repeated at 5 Hz.

In the warm option it is not necessary to separately measure the energy deposited in each of the 192 bunches as the average occupancy in our very granular detector, integrated over the bunch train, will be much less than 1% in almost all of the detector and approach 1% in the forward and backward endcaps. Since the total length of the bunch train is approximately 250 ns, it is possible to integrate the charge of each pixel over the entire bunch train. It is, however, necessary to tag the time of the energy deposition with enough precision to allow the time of each shower or track to be estimated with a precision of better than 1 to 2 ns. For charged hardons we expected to have at least 30 minimum ionizing (or larger) samples which implies that the time of arrival of the energy in each layer must be measured to about 5 ns. For electromagnetic showers we will have several pixels with large energy depositions which can individually be measured with a precision of 1 ns.

In the cold option the integrated bunch-train occupancies are a factor of 20 higher and the total time of the bunch train is almost 1 ms. The high occupancy and the long length of the bunch train will require some kind of buffering of the charge signals and the time of the associated beam crossing. Because of the 337 ns between bunches in the cold option a precision timing measurement is not needed to associate the deposited energy to the beam crossing.

Given that the International Technology Recommendation Panel (ITRP) has recently recommended that the world community proceed with a linear collider based on cold technology, we are presently adapting our previous work on an ASIC for warm technology to a configuration for the cold technology. The requirements imposed by the silicon detectors themselves are similar for both "cold" and "warm" designs. The ten prototype detectors we have in hand will work for tests of the cold electronics.

In this paper we concentrate on the test of the prototypes and studies of timing resolution. The work on timing resolution may not be relevant for the "cold" detector configuration. It is possible that time tagging may be useful for tagging energy deposited in the detector from looping tracks and other background that will occur out-of-time. Furthermore timing in silicon detectors is useful in other applications [5].

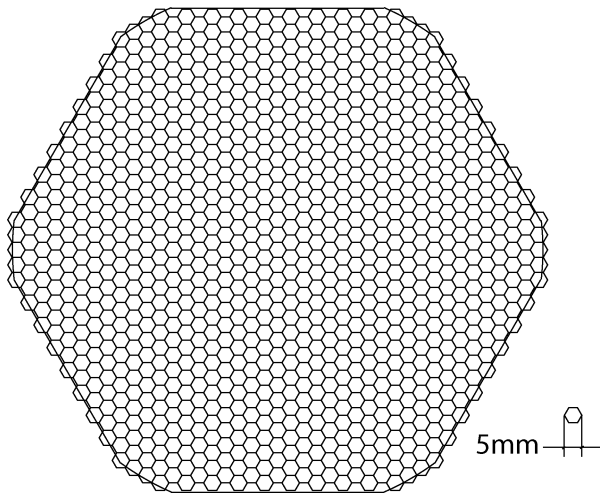

Fig. 3. Layout of 1024 pixels on a hexagonal detector based on 6 in wafers.

II. Silicon Detector Prototypes

The silicon detectors [6] are designed to make maximal use of the available area on 15 cm (6 in) silicon wafers. The detectors are divided into approximately 750 5 mm pixels as shown in Fig. 3. Each pixel consists of a diode formed by p^+ implant in the high resistivity wafers which have been thinned to 300 $\mu\mathrm{m}$. The p^+ implant is directly covered by a layer of Al making the detectors DC coupled. Each of the pixels are connected to the bump-bonding array at the center of the wafer by traces on a second metal layer separated by approximately 0.9 $\mu\mathrm{m}$ of insulation. Bias is applied to the metal layer on the back side of the detector.

The hexagonal pixels have a long dimension of 5 mm and area of 16.24 mm^2 giving an expected detector capacitance of approximately 5.7 pF. The total capacitance seen by the read-out electronics will be dominated by the stray capacitance associated with traces that connect pixels with the bump-bond array. Since detector noise and timing resolution will depend critically on the capacitance, it is important to verify that their values agree with calculations based on the geometry of the detectors.

We have measured the values of stray capacitance of five pixels located near the outer edge of the detector. The capacitance was measured by contacting a probing pad located in the bump-bond array with a tungsten probe. The backside of the

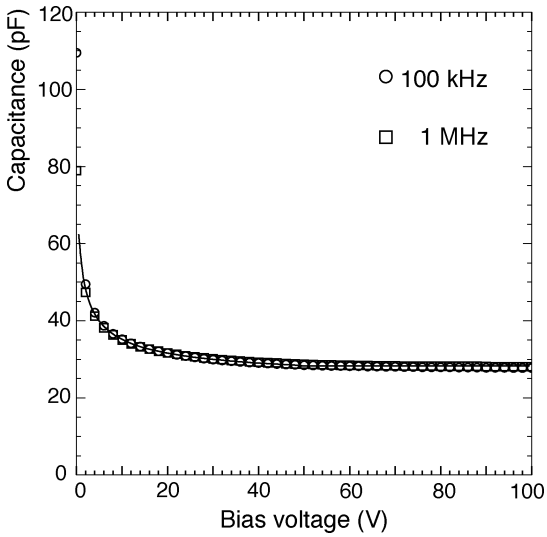

Fig. 4. Measured capacitance versus voltage for a single pixel.

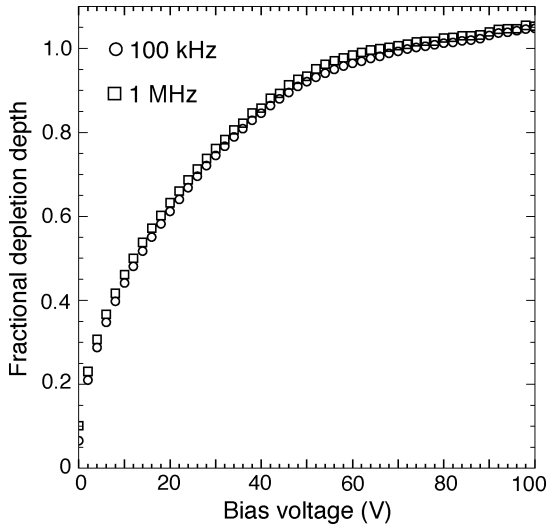

Fig. 5. Relative depletion depth as a function of voltage.

TABLE I
MEAN STRAY CAPACITANCE MEASUREMENT
OBTAINED FROM A FIT TO THE CV CURVE

Expected	Measured (100kHz)	Measured (1 MHz)
23.0 ± 0.2 pF	21 ± 1 pF	22 ± 1 pF

detector was then biased with voltage V_{bias} to measure the CV curve. The remaining pixels in the detector were left floating. Because of the large capacitances of the floating pixels, which are not depleted, they will essentially appear as grounds to thetraces which connect the bump-bonding array to the pixel under test.

A typical CV curve is shown in Fig. 4. The superimposed curve is of the form

$$\begin{aligned} C_{tot} &= C_{stray} + C_{geom}\sqrt{\tfrac{V_{dep}+V_{bi}}{V_{bias}+V_{bi}}} \quad V_{bias} < V_{dep} \\ C_{tot} &= C_{stray} + C_{geom} \qquad\qquad\qquad\quad V_{bias} > V_{dep} \end{aligned}$$

where C_{tot} is the predicted total capacitance, C_{stray} is the stray capacitance, V_{dep} is the depletion voltage and V_{bi} is the built-in voltage. It is not possible to reliably extract all of these parameters from a fit. We fix $C_{geom} = 5.7$ pF and fit for C_{stray}, V_{dep} and V_{bi} with the requirement that V_{bi} be consistent with V_{dep} and the expected doping concentration of the p^+ implant. The resulting mean value of C_{stray} is given in Table I. The resulting fitted values of V_{dep} are between 40 and 55 V. Note that surrounding pixels were not held at ground and the measured capacitance may include a contribution from fringe fields. The differences seen between capacitance measurements at 100 kHz and 1 MHz at very low bias voltage have little effect on the fitted values of C_{stray} [7].

Another way of looking at the same data is shown in Fig. 5. Here the quantity

$$d = \frac{C_{geom}}{C_{measured} - C_{stray}}$$

is plotted where $C_{geom} = 5.7$ pF and C_{stray} is the fitted value of the stray capacitance. The continued increase in d as V_{bias} is increased above the fitted value of V_{dep} is probably due to the effects of the floating neighboring pixels.

The values of the stray capacitance are compared to their expected value based on the measured length of the traces and the number of other traces which cross the pixels. Note that pixels near the center of the wafer have a large contribution to their stray capacitance from traces that connect to other pixels at larger radius. Pixels at the outer edges of the detector have a large contribution to their stray capacitance from the long traces that connect them to the bump-bond array and a small contribution from the traces connecting other pixels to the bump-bond array. The two effects nearly compensate each other. The expected value of the stray capacitance is in good agreement with the measured values in Table I.

We have also measured the resistance of one of the traces connecting the pixel to the bump-bond array. The measured resistance is $(57 \pm 2)\Omega/\mathrm{cm}$ and is somewhat larger than the value for pure aluminum traces with cross section of 1 μm by 6 μm of 47 Ω/cm.

The stray capacitance and resistance are sufficiently small to allow good minimum ionizing performance of our detectors. In future versions of the prototype detectors we will optimize the routing of the traces to the pixels as well as the thickness of the oxide layer and width of the traces in order to minimize power consumption of the electronics and the total cost of the electronics and detectors.

III. TIMING MEASUREMENTS

In order to explore the feasibility of timing measurements at the level needed for the warm machines, we have used DC coupled silicon detectors similar to our LC prototype. One of these detectors [8] has a small window in the metallization to allow a focused beam from a 1064 nm IR laser to simulate minimum ionizing tracks. The IR laser is used so that electron-hole pairs will be produced throughout the 300 μm depth of the silicon detectors, rather than just at the surface as would be the case for a visible laser. The set up was similar to that used in [9]. For these measurements the laser was focussed to a spot with a diameter

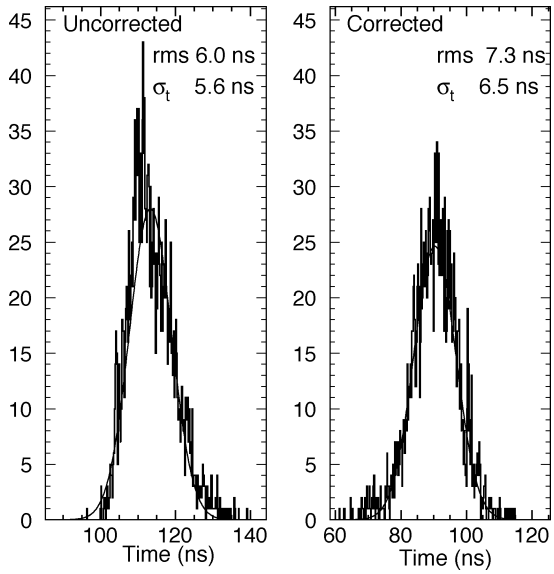

Fig. 6. Timing resolution for 0.5 MIP laser pulses, $V_{bias} = 120$ V.

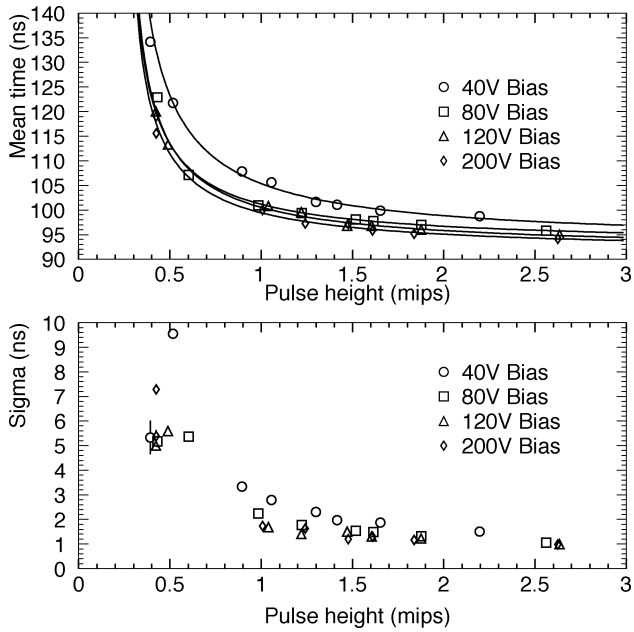

Fig. 7. Timing mean and sigma as a function of laser pulse size.

of approximately 10 μ using an IR microscope objective. The full width of the laser pulse was set to 0.8 ns.

These measurements are based around an Alessi 3200 A manual probe station which allows us to test silicon detectors without permanently bonding to them. Contact is made to the front side of the detector using tungsten probes. The signals from the silicon pads are connected to $\sim$ 20 cm 50 Ω coax cables, with capacitance measured as 23 pF, that bring the signals to the charge amplifiers. The bias voltage is applied to the back side of the detectors using an insulated brass vacuum chuck.

For these measurements we used AMPTEK 250 F charge amplifiers with an IFN152 input FET. The input FET was operated with 2.75 mA drain current. The output impedance of the AMPTEK is $\sim 100\,\Omega$ and can not drive long $50\,\Omega$ cables. Each AMPTEK was connected with ~ 5 cm $50\,\Omega$ cables AC coupled to an OPA687U op-amp based shaper which drive the cables to the Tektronix 3054B oscilloscope. The capacitance of a typical detector element, $\sim$ 15 pF, when combined with the 23 pF cables, is 38 pF, considerably more than that from the LC prototype pads furthest from the readout electronics.

In addition to studying laser pulses we have also used cosmic ray muons. A second silicon detector was mounted on a metal tray to provide bias and read out via traces on a circuit board that were connected to the detector elements with conductive epoxy. The tray was designed to allow the detector to be mounted under the vacuum chuck. Including cables, a typical detector element had a capacitance of 53 pF. In addition, the presence of a cosmic ray muon was confirmed by using two large slabs of scintillator located under the probe station.

For each laser pulse the time at which the oscilloscope trace crossed a threshold corresponding to 0.35 MIPs was recorded. (Here, and in what follows, a MIP is taken as the mean of the measured charge distribution from triggered cosmic rays.) The resulting timing resolution for laser pulse amplitudes corresponding to 0.5 MIPs is shown in Fig. 6. The fitted mean and sigma of these pulses are shown in Fig. 7 as function of laser pulse size and bias voltage. The curves assume the front edge of the pulse can be parameterized as $v(t) = v_0(1-e^{-t/\tau})$ where τ is a free parameter. The resulting values of τ are given in Table II. The errors are statistical only.

TABLE II
TIME CONSTANT τ FOR VARIOUS VALUES OF BIAS VOLTAGE

Bias voltage	τ	Theoretical collection time	
		electrons	holes
40 V	37.5 ± 0.2 ns	-	-
80 V	25.6 ± 0.1 ns	8.2 ns	25.6 ns
120 V	27.3 ± 0.1 ns	5.2 ns	15.9 ns
200 V	25.1 ± 0.1 ns	3.0 ns	9.3 ns

Using the value of τ for each bias voltage a time walk correction can be applied to get the results shown in Fig. 8. To demonstrate that good resolution can be obtained for cosmic rays, we consider coincidences between two silicon detectors and the scintillators. The bias voltage was set to 120 V. The charge in each silicon detector was required to be larger than 0.58 MIPS. The resulting time resolution (difference/$\sqrt{2}$) is shown in Fig. 9. The rms is $\sigma_t = 3.4 \pm 0.4$ ns. The 27 ns shaping time of the laboratory system was perhaps somewhat faster than could be obtained in an ASIC. Adding an additional band width limitation to reduce τ to 37 ns, the resulting cosmic timing resolution was $\sigma_t = 4.2 \pm 0.5$ ns, still consistent with our 5 ns goal.

Finally we note that timing resolution for individual large pulses is quite good. For example, a 1 GeV photon will almost always have at least one layer with energy deposition corresponding to 6 MIPs or more. Our resolution for 6 MIP laser pulses is approximately 0.6 ns as shown in Fig. 10.

A. Monte Carlo Simulation

The timing measurements of nonshowering hadrons in the calorimeter can be determined from the average of the time measurement in each layer of the calorimeter. The timing resolution

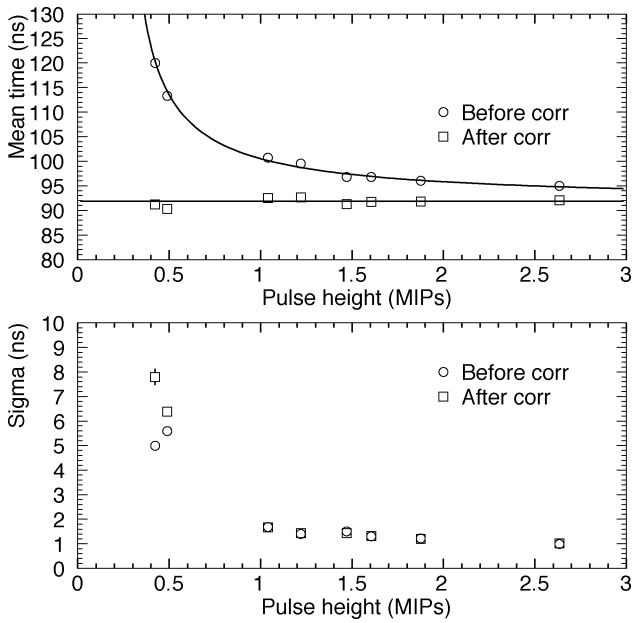

Fig. 8. Timing mean and sigma as a function of laser pulse size before and after correction, $V_{bias} = 120\ \mathrm{V}$.

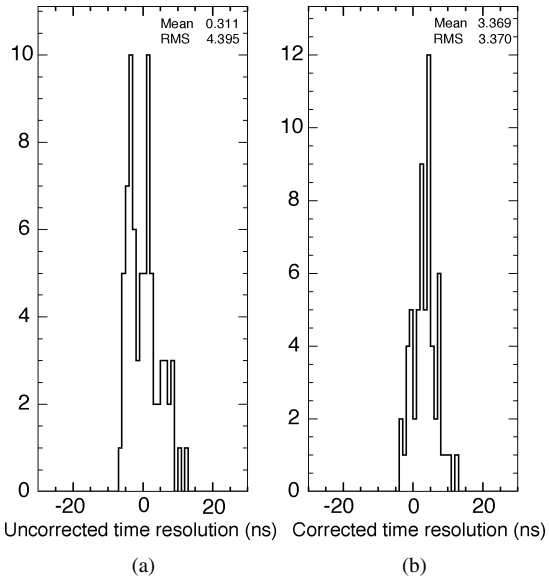

(a) (b)

Fig. 9. Timing resolution for comic rays (a) before time walk correction and (b) after.

will vary as a function of position of the particles as they traverse the layers of the calorimeter. The position of the wafers in successive layers will not be projective so each hadron will get a mix of measurements with different trace resistances and stray capacitances. In our simple Monte Carlo model we parameterize the expected series resistance and stray trace capacitances as a function of distance to the readout chip. We then randomly distribute the hits over the area of the silicon detectors. The simulation also models the Landau fluctuations of the charge deposited in the silicon detectors. The model assumes a trace resistance of 350 Ω and a trace capacitance of 15 pF for the longest traces. These parameters are somewhat better than those achieved in the first prototype detectors, but could be achieved by thickening the

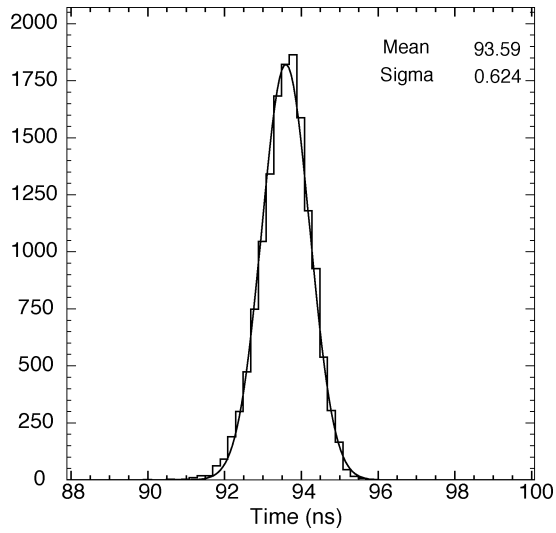

Fig. 10. Timing resolution for 6 MIP laser pulses, typical of GeV photon energy depositions.

oxide layer and the second metal layer and by using traces which take a more direct route to the pixels. The rising edge of the electronics output signal was modeled by a waveform with single exponential with time constant $\tau = 50$ ns. The threshold for the timing measurement corresponded to 0.33 MIPs (8000 electrons). Noise from the series resistance of the traces, the input FET and an "excess noise" contribution equal to that of the input FET with transconductance $g_m = 1.5\ \mathrm{mS}$ were included. Other details of the simulation can be found in [3].

To determine the timing resolution for hadrons that cross all 30 layers of the calorimeter, the time in each layer was corrected for pulse height using a simulation of the charge measurement and then the average was calculated using a truncated mean algorithm. The resulting time resolution was 0.72 ns. A timing measurement with this resolution would be adequate to associate the tracks to beam crossings in the warm machine. In a detector for a cold machine it would also be adequate for tagging energy depositions from looping tracks that have time delays of greater than 2 ns.

IV. Conclusion

We have made measurements of the stray capacitance and resistivity associated with the trace lines on large silicon detectors with 5 mm hexagonal pixels. The measurements agree with expectations based on the detector geometry and have suitable values for use in an LC fine grained calorimeter.

We have also used similar pad detectors to measure the timing resolution with electronics that have similar properties to that foreseen for use in an LC fine grained calorimeter.

Acknowledgment

The authors wish to thank T. Neely and E. Fitzgerald for assisting in making the measurements reported here. The authors also wish to thank K. Johnson of the University of Oregon mechanical shop and C. Dax of the University of Oregon electronics shop.

REFERENCES

[1] J. Brau, A. Arodzero, and D. Strom, "Calorimetry for the NLC Detector," in *Proc. 1996 DPF/DPB Summer Study on New Directions in High-Energy Physics*, 1997, pp. 437–441.

[2] H. Videau and J. C. Brient, "A Si-W calorimeter for linear collider physics," in *Proc. 10th Int. Conf. Calorimetry in High Energy Physics (CALOR 2002)*, Pasadena, CA, pp. 309–320.

[3] D. Strom, R. Frey, M. Breidenbach, D. Freytag, N. Graf, G. Haller, O. Milgrome, and V. Radeka, "Design and development of a dense, fine grained silicon tungsten calorimeter with integrated electronics," in *Proc. XI Int. Conf. Calorimeters in High Energy Physics*, Perugia, Italy, 2004, to be published.

[4] R. Frey, D. Strom, M. Breidenbach, D. Freytag, N. Graf, G. Haller, O. Milgrome, and V. Radeka, "Silicon/tungsten ECal for SiD—status and progress," in *Proc. Int. Conf. Linear Colliders, (LCWS 2004)*, Paris, France, to be published.

[5] A. Castoldi, A. Galimberti, E. Gatti, C. Guazzoni, P. Rehak, and L. Strüder, "Self-triggered multi-linear silicon drift detector," IEEE Trans. Nucl. Sci., to be published.

[6] Hamamatsu Photonics, Hamamatsu City, Japan.

[7] R. Wunstorf, M. Benkert, N. Claussen, N. Croitoru, E. Fretwurst, G. Lindström, and T. Schulz, "Results on radiation hardness of silicon detectors up to neutron fluences of $10^{15}\ \mathrm{n/cm^2}$," *Nucl. Instrum. Methods Phys. Res. A*, vol. 315, pp. 149–155, 1992.

[8] G. Abbiendi *et al.*, "Precision luminosity for Z^0 lineshape measurements with a silicon-tungsten calorimeter," *Eur. J. Phys.*, vol. 14, pp. 373–425, 2000.

[9] R. T. Kollipara, A. Arodzero, G. Bashindzhagain, J. E. Brau, R. Frey, D. Gao, D. Mason, N. Sinev, D. Strom, and X. Yang, "Study of 18-cm long single sided AC coupled silicon microstrip detectors," *IEEE Trans. Nucl. Sci.*, vol. 42, no. 2, pp. 92–101, Apr. 1995.